*Journal of Sound and Vibration* (1998) **216**(4), 585–600
*Article No*. sv981715

# THE DIRECTIONAL WIGNER DISTRIBUTION AND ITS APPLICATIONS

C. W. Lee and Y.-S. Han

*Center for Noise and Vibration Control* (*NOVIC*), *Department of Mechanical Engineering*, *KAIST*, *Science Town*, *Taejon* 305-701, *South Korea*

(*Received* 7 *March* 1997, *and in final form* 23 *March* 1998)

A new signal processing technique, the directional Wigner distribution (dWD), is presented to characterize the instantaneous planar motion of a measurement point in a structure from its transient complex-valued vibration signal. It is proven that the auto-dWD essentially tracks the shape and directivity of the instantaneous planar motion, whereas the phase of the cross-dWD indicates its inclination angle. Finally, the technique is successfully applied to two practical cases: a rotor during run-up and an automobile engine during crank-on/idling/engine-off.



## 1. INTRODUCTION

Spectral analysis using the FFT algorithm is perhaps the most popular signal processing technique used for monitoring the vibration signals associated with mechanical failures or faults in machines because the frequency components and the corresponding amplitudes vary in accordance with various fault mechanisms. However, when the basic nature of signals changes with time, spectral analysis often yields poor results due to spectral smearing. Response signal of a rotor as a function of rotational speed during start-up or shut-down is a good example. In particular, this approach is not really valid for transient signals resulting from shaft rubs in journal bearings and spalls in rolling element bearings, if time-localized spectral results are required. Thus, there has been a great need to represent time-varying signals in the time–frequency domain. A traditional tool for the analysis of time-varying signals has been the short-time Fourier transform, which is commonly called the spectrogram. The spectrogram is typically obtained by applying a fixed length, moving window to the time-varying data sequence prior to computing the spectrum. Its length is chosen by considering the tradeoff between the time and frequency resolutions obtainable. An efficient time–frequency representation that aims at overcoming the tradeoff problem is the Wigner distribution (WD) [1–5], which has been widely applied in the areas of optics [6], speech analysis [7], structure-borne noise identification [8, 9] and machinery condition monitoring [10–13]. The WD which conventionally deals with the real valued time-varying signals is well documented in the literature [3], compared with other joint time–frequency methods. Among others, the major deficiency of the WD is the so-called presence of interference terms. In addition,

0022–460X/98/390585 + 16 $30.00/0 

the WD of discrete time signals suffers from the aliasing problem, which may be overcome by employing various schemes [2, 14]. In this work, the auto- and cross-directional Wigner distributions (dWDs) are introduced to account for complex-valued time varying signals, which represent the planar motion of the measurement points in structures at each instant of time. The auto- and cross-dWDs are defined such that they carry the information on the shape and directivity, and the inclination angle, respectively, of the instantaneous planar motion. The dWD has the problems and remedies similar to the conventional Wigner distribution. The aliasing problem and the interference terms between the forward and backward harmonic components are avoided by transforming a complex-valued signal into the forward and backward pass analytic signals. The reduction of the interference terms associated with multiple harmonic components and the elimination of possible negative values are achieved by convolving the dWD with a Gaussian window function. A numerical example and two practical applications are treated to demonstrate the effectiveness of the dWD in characterizing transient complex-valued signals.

## 2. COMPLEX NOTATION

In this section, the convention for representing complex signals will be established and the complex harmonic components as phasors rotating in a complex plane considered [15–17]. Let one first consider a pair of complex conjugate signals, $p(t)$ and $\bar{p}(t)$, of the form

$$p(t) = y(t) + \mathrm{j}z(t), \qquad \bar{p}(t) = y(t) - \mathrm{j}z(t), \tag{1}$$

where $y(t)$ and $z(t)$ are the real signals, j $(=\sqrt{-1})$ means the imaginary number and the bar denotes the complex conjugate. It is then natural to associate the complex signal $p(t)$ with a moving point, or a moving vector drawn from the origin, in the plane whose cartesian co-ordinates are $y(t)$ and $z(t)$. By displaying the complex signal $p(t)$ geometrically in the complex plane, the $y$-axis becomes the real axis, the $z$-axis being the imaginary axis, as indicated in Figure 1. The complex harmonic signal $p(t)$ of frequency $\omega$ can be rewritten in polar form, using Euler's formula [15], as

$$\begin{aligned} p(t) &= p^f(t) + p^b(t) = r^f \mathrm{e}^{\mathrm{j}\omega t} + r^b \mathrm{e}^{-\mathrm{j}\omega t} \\ &= \{\tfrac{1}{2}(y_c + z_s) + (\mathrm{j}/2)(z_c - y_s)\} \mathrm{e}^{\mathrm{j}\omega t} + \{\tfrac{1}{2}(y_c - z_s) + (\mathrm{j}/2)(z_c + y_s)\} \mathrm{e}^{-\mathrm{j}\omega t}, \end{aligned} \tag{2}$$

where, $r^f = |r^f| \mathrm{e}^{\mathrm{j}\phi^f}$, $r^b = |r^b| \mathrm{e}^{\mathrm{j}\phi^b}$, and using the relation $p(t) = y(t) + \mathrm{j}z(t)$,

$$y(t) = y_c \cos \omega t + y_s \sin \omega t, \qquad z(t) = z_c \cos \omega t + z_s \sin \omega t. \tag{3}$$

Here the superscripts $b$ and $f$ denote the backward (clockwise) and forward (counter-clockwise in Figure 1), and, $y_c$ and $y_s$($z_c$ and $z_s$) are the Fourier coefficients associated with $y(t)$($z(t)$). Note that the complex term $\mathrm{e}^{\mathrm{j}\omega t}$ ($\mathrm{e}^{-\mathrm{j}\omega t}$) is associated with the forward (backward) rotating unity vector at the circular rotating speed of $\omega$ and that the complex quantity $r^f$ ($r^b$) is associated with the vector having the amplitude, $|r^f|$ ($|r^b|$), and the initial phase, $\phi^f$ ($\phi^b$). It is well known

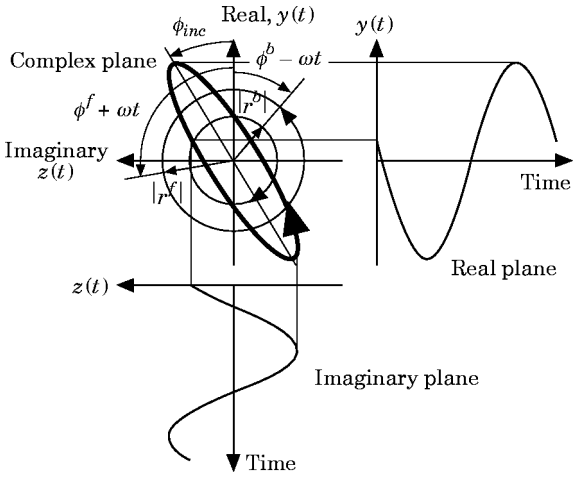


Figure 1. Representation of a complex-valued signal as the sum of two contra-rotating vectors.

that the complex harmonic signal, which is the resultant of two contra-rotating vectors, each with different amplitudes and initial phases, forms an ellipse in the complex plane [15]. The shape and directivity of the elliptic planar motion are determined as follows:

$$r^f\ (r^b) = 0\text{: backward (forward) circular planar motion,}$$

$$|r^b| > |r^f|\text{: backward elliptic planar motion,}$$

$$|r^b| = |r^f|\text{: straight line motion,}\quad |r^b| < |r^f|\text{: forward elliptic planar motion.} \tag{4}$$

To quantify the above shape and directivity information, the shape and directivity index (SDI) is introduced and defined as

$$-1 \leqslant \mathrm{SDI} = (|r^f| - |r^b|)/(|r^f| + |r^b|) \leqslant 1 \tag{5}$$

where the inequality relations can be easily proven. Note that

$$\mathrm{SDI} = -1\text{: backward circular planar motion,}$$

$$-1 < \mathrm{SDI} < 0\text{: backward elliptic planar motion,}$$

$$\mathrm{SDI} = 0\text{: straight line motion,}$$

$$0 < \mathrm{SDI} < 1\text{: forward elliptic planar motion,}$$

$$\mathrm{SDI} = 1\text{: forward circular planar motion.}$$

In other words, the sign of the SDI determines the directivity and the absolute value of the SDI indicates the roundness (the correlation coefficient to a circle).

The inclination angle $\phi_{inc}$ of the ellipse made by the major axis of the ellipse with respect to the $y$-axis is obtained as

$$\phi_{inc} = \tfrac{1}{2}(\phi^f + \phi^b). \tag{6}$$

Therefore, in order to identify the parameters of the elliptic planar motion, one needs to acquire the shape, directivity and inclination angle of the planar motion.

## 3. HILBERT TRANSFORM

### 3.1. DEFINITION

The conventional analytic signal associated with a real signal is defined such that its imaginary part is the Hilbert transform of the real signal, so that its spectrum is zero over the negative (backward) frequency region [18]. The use of the conventional analytic signal can be considered as the forward pass transformation of the original real signal in the sense that it only passes the forward (positive) harmonic components. The backward pass transformation can be similarly designed by using the complex conjugate of the analytic signals. When one deals with real signals, the forward and backward pass transformations result in identical spectra except the sign of frequency. But the spectrum of a complex-valued signal, in general, shows the two-sided frequency contents, which are different over the positive and negative frequency ranges. Therefore, it is necessary to define the forward and backward pass analytic signals of a complex-valued signal.

Since the Hilbert transform is a linear operator, the Hilbert transform of a complex-valued signal $p(t)$ is another complex-valued signal $\tilde{p}(t)$, i.e.

$$\tilde{p}(t) = \int_{-\infty}^{\infty} \frac{p(u)}{\pi(t-u)}\,\mathrm{d}u = p(t)*(1/\pi t). \tag{7}$$

The above Hilbert transform is the convolution of the complex signal $p(t)$ with $1/(\pi t)$. Let $\tilde{P}(\omega)$ denotes the Fourier transform of $\tilde{p}(t)$, then according to the convolution theorem,

$$\tilde{P}(\omega) = P(\omega)B(\omega). \tag{8}$$

where $B(\omega)$ is the Fourier transform of $1/(\pi t)$, i.e.,

$$B(\omega) = -\mathrm{j}\ \mathrm{sgn}\ (\omega), \tag{9}$$

with

$$\mathrm{sgn}\ (\omega) = \begin{Bmatrix} 1, & \text{for } \omega > 0, \\ 0, & \text{for } \omega = 0, \\ -1, & \text{for } \omega < 0, \end{Bmatrix}$$

The magnitude and the phase shift of $B(\omega)$ are found to be

$$|B(\omega)| = 1, \qquad \phi_B(\omega) = \begin{Bmatrix} \pi/2 & \text{for } \omega > 0 \\ -\pi/2 & \text{for } \omega < 0, \end{Bmatrix} \tag{10}$$

implying that $B(\omega)$ is a $90^\circ$ phase shift system. Hence, the Hilbert transformed signal can be obtained by multiplying positive and negative frequency components by $-\mathrm{j}$ and j, respectively, in the frequency domain.

### 3.2. ANALYTIC SIGNALS ASSOCIATED WITH COMPLEX-VALUED SIGNALS

An analytic signal associated with a complex-valued signal can be defined so that it consists of the complex-valued original signal and its Hilbert transformed signal. With a time signal $p(t)$ and its Hilbert transform $\tilde{p}(t)$, the forward and backward pass analytic signals, $p^f(t)$ and $p^b(t)$, associated with $p(t)$ can be defined as

$$p^f(t) = \{p(t) + \mathrm{j}\tilde{p}(t)\}/2, \qquad p^b(t) = \{p(t) - \mathrm{j}\tilde{p}(t)\}/2. \tag{11}$$

The corresponding Fourier transforms, $P^f(\omega)$ and $P^b(\omega)$ become

$$P^f(\omega) = [P(\omega) + \mathrm{sgn}\,(\omega)P(\omega)]/2 = \begin{Bmatrix} P(\omega), & \text{for } \omega > 0, \\ P(\omega)/2, & \text{for } \omega = 0, \\ 0, & \text{for } \omega < 0, \end{Bmatrix} \tag{12a}$$

$$P^b(\omega) = \begin{Bmatrix} 0, & \text{for } \omega > 0, \\ P(\omega)/2, & \text{for } \omega = 0, \\ P(\omega), & \text{for } \omega < 0. \end{Bmatrix} \tag{12b}$$

Note that the forward (backward) pass analytic signal only includes the positive (negative) frequency components.

## 4. DIRECTIONAL WIGNER DISTRIBUTION

### 4.1. DEFINITION AND PROPERTIES

In this section, the conventional Wigner distribution is extended to account for complex-valued signals by introducing dWD, and the properties of dWD are examined.

By simply replacing the real-valued signal in the conventional definition of WD by the complex-valued signal, one may define the auto- and cross-WDs, $W_p(t, \omega)$ and $W_{\tilde{p},p}(t, \omega)$ of a complex-valued signal $p(t) = y(t) + \mathrm{j}z(t) = p^f(t) + p^b(t)$ as in reference [2] as

$$\begin{aligned} W_p(t, \omega) = W_{p,p}(t, \omega) &= \int_{-\infty}^{\infty} \mathrm{e}^{-\mathrm{j}\omega\tau} \tilde{p}\left(t - \frac{\tau}{2}\right) p\left(t + \frac{\tau}{2}\right) \mathrm{d}\tau \\ &= W_{p^f,p^f}(t, \omega) + W_{p^b,p^b}(t, \omega) + W_{p^f,p^b}(t, \omega) + W_{p^b,p^f}(t, \omega), \end{aligned} \tag{13a}$$

$$\begin{aligned} W_{\tilde{p},p}(t, \omega) &= \int_{-\infty}^{\infty} \mathrm{e}^{-\mathrm{j}\omega\tau} p\left(t - \frac{\tau}{2}\right) p\left(t + \frac{\tau}{2}\right) \mathrm{d}\tau \\ &= W_{\tilde{p}^f,p^b}(t, \omega) + W_{\tilde{p}^b,p^f}(t, \omega) + W_{\tilde{p}^f,p^f}(t, \omega) + W_{\tilde{p}^b,p^b}(t, \omega), \end{aligned} \tag{13b}$$

where $W_{p^f,p^f}(t, \omega)$ and $W_{p^b,p^b}(t, \omega)$ ($W_{\tilde{p}^f,p^b}(t, \omega)$ and $W_{\tilde{p}^b,p^f}(t, \omega)$) contain, in addition to the desired signal terms, the undesired interference terms between multi-harmonic components. On the other hand, $W_{p^f,p^b}(t, \omega)$ and $W_{p^b,p^f}(t, \omega)$

($W_{\bar{p}^f,p^f}(t,\omega)$ and $W_{\bar{p}^b,p^b}(t,\omega)$) are the interference terms between the forward and backward harmonic components. Note that by definition, the Wigner kernels $\bar{p}(t-\tau/2)p(t+\tau/2)$ and $p(t-\tau/2)p(t+\tau/2)$ are the conjugate even and even functions of $\tau$, respectively. Especially, from definition (13), it holds

$$W_p(t,\omega) = \bar{W}_p(t,\omega), \qquad W_{\bar{p},p}(t,\omega) = W_{\bar{p},p}(t,-\omega) = \bar{W}_{p,\bar{p}}(t,\omega). \quad (14a, b)$$

In other words, the auto-WD, which is the Fourier transform of the conjugate even Wigner kernel with respect to $\tau$, is real, but not always positive, whereas the cross-WD, which is the Fourier transform of the even Wigner kernel with respect to $\tau$, is an even, but not real in general, function of $\omega$.

On the other hand, the auto- and cross-dWDs of a complex-valued signal $p(t)$ are defined with the forward and backward pass analytic signals, respectively, as

$$W_p^{\mathrm{d}}(t,\omega) = \begin{cases} W_{p^f}(t,\omega) \\ W_{p^b}(t,\omega) \end{cases} = \begin{cases} \displaystyle\int_{-\infty}^{\infty} \mathrm{e}^{-\mathrm{j}\omega\tau} \bar{p}^f\left(t-\frac{\tau}{2}\right) p^f\left(t+\frac{\tau}{2}\right) \mathrm{d}\tau, & \text{for } \omega > 0, \\ \displaystyle\int_{-\infty}^{\infty} \mathrm{e}^{-\mathrm{j}\omega\tau} \bar{p}^b\left(t-\frac{\tau}{2}\right) p^b\left(t+\frac{\tau}{2}\right) \mathrm{d}\tau, & \text{for } \omega < 0, \end{cases} \quad (15a)$$

$$W_{\bar{p},p}^{\mathrm{d}}(t,\omega) = W_{\bar{p}^b,p^f}(t,\omega) = \int_{-\infty}^{\infty} \mathrm{e}^{-\mathrm{j}\omega\tau} p^b\left(t-\frac{\tau}{2}\right) p^f\left(t+\frac{\tau}{2}\right) \mathrm{d}\tau, \quad \text{for all } \omega, \quad (15b)$$

which state that by separating the backward or forward components, one can remove the interference terms between the forward and backward components. Thus, for complex-valued signals, the dWDs defined in equation (15) are far less contaminated by undesired interference terms than the WDs in equation (13). In addition, the dWD defined by using the analytic signal can eliminate the aliasing problem [5].

To demonstrate some important properties of auto- and cross-dWDs, one considers a complex chirp signal, whose instantaneous frequency increases linearly with time; i.e.,

$$p(t) = r^f \mathrm{e}^{\mathrm{j}\alpha t^2/2} + r^b \mathrm{e}^{-\mathrm{j}\alpha t^2/2}, \quad (16)$$

where $r^f = |r^f| \mathrm{e}^{\mathrm{j}\phi^f}$, $r^b = |r^b| \mathrm{e}^{\mathrm{j}\phi^b}$. Here $\alpha$ is a constant. From equation (15), one obtains the corresponding auto-dWD as

$$W_p^{\mathrm{d}}(t,\omega) = \begin{cases} 2\pi\{|r^f|^2\delta(\omega-\alpha t)\}, & \text{for } \omega > 0, \\ 2\pi\{|r^b|^2\delta(\omega+\alpha t)\}, & \text{for } \omega < 0. \end{cases} \quad (17)$$

It implies that the auto-dWD of the complex chirp signal is concentrated at any instant around the instantaneous forward (positive) and backward (negative)

frequencies, $+\alpha t$ and $-\alpha t$, respectively, in the time–frequency plane. This is one of the main motivations for its use. On the other hand, the cross-dWD becomes

$$W^{\mathrm{d}}_{\bar{p},p}(t,\omega) = 2\pi\{|r^f\|r^b|\,\mathrm{e}^{\mathrm{j}\phi^f}\,\mathrm{e}^{\mathrm{j}\phi^b}[\delta(\omega-\alpha t)]\}. \tag{18}$$

Note that the auto- and cross-dWDs remove the undesired interference term between the forward and backward components. The instantaneous inclination angle can be defined, from the phase of the cross-dWD, as

$$\tan\{2\phi_{inc}(t,\omega)\} = \mathrm{Im}\{W^{\mathrm{d}}_{\bar{p},p}(t,\omega)\}/\mathrm{Re}\{W^{\mathrm{d}}_{\bar{p},p}(t,\omega)\}. \tag{19}$$

Thus, the instantaneous inclination angle can be expressed as

$$\phi_{inc}(t,\omega) = \tfrac{1}{2}[\phi^f + \phi^b]. \tag{20}$$

### 4.2. SMOOTHED DIRECTIONAL WIGNER DISTRIBUTION

Even if the dWD is theoretically attractive, the practical application of the dWD is often restricted by the presence of the interference terms. An improvement in the attenuation of interference terms can be made by the convolution with a smoothing function in the time-frequency domain [3, 19]. The Gaussian window function is commonly used as a smoothing function:

$$G(t,\omega) = (2\pi\sigma_t\sigma_w)^{-1}\exp[-(t^2/2\sigma_t^2 + \omega^2/2\sigma_\omega^2)], \tag{21}$$

where the positive constants $\sigma_t = M\Delta_t$ and $\sigma_\omega = N\Delta_\omega$ indicate the extent of smoothing in the time and frequency directions, $\Delta_t$ and $\Delta_\omega$ denote the corresponding resolutions, respectively, and, $M$ and $N$ are the integer numbers. The smoothed auto- and cross-dWDs can be defined as

$$\tilde{W}^{\mathrm{d}}_{p}(t,\omega) = \frac{1}{2\pi}\int_{-\infty}^{\infty}\int_{-\infty}^{\infty} W^{\mathrm{d}}_{p}(t',\omega')G(t-t',\omega-\omega')\,\mathrm{d}t'\,\mathrm{d}\omega', \tag{22a}$$

$$\tilde{W}^{\mathrm{d}}_{\bar{p},p}(t,\omega) = \frac{1}{2\pi}\int_{-\infty}^{\infty}\int_{-\infty}^{\infty} W^{\mathrm{d}}_{\bar{p},p}(t',\omega')G(t-t',\omega-\omega')\,\mathrm{d}t'\,\mathrm{d}\omega'. \tag{22b}$$

Note that the smoothing operation yields the positive smoothed dWD when $\sigma_t\sigma_\omega \geqslant 0{\cdot}5$ [20]. Unfortunately, this attenuation of interference terms comes at the cost of a loss of time–frequency concentration. Therefore, there exists a fundamental tradeoff between good interference terms attenuation and good time–frequency concentration. Also, the smoothed dWD tends to lose most of the attractive mathematical properties of the defined dWD [3].

One can also define the instantaneous SDI of the time varying complex harmonic component by using the smoothed auto-dWD, i.e.,

$$-1 \leqslant \mathrm{SDI}(t) = (|r^f(t)| - |r^b(t)|)/(|r^f(t)| + |r^b(t)|) \leqslant 1, \tag{23}$$

where

$$|r^f(t)| = \sqrt{\frac{1}{2\pi}\int_{\omega_1}^{\omega_2}\tilde{W}^{\mathrm{d}}_{p}(t,\omega)\,\mathrm{d}\omega}, \qquad |r^b(t)| = \sqrt{\frac{1}{2\pi}\int_{-\omega_2}^{-\omega_1}\tilde{W}^{\mathrm{d}}_{p}(t,-\omega)\,\mathrm{d}\omega}.$$

Here $\omega_1$ and $\omega_2$ form a frequency band near the spectral peak of interest. Note that the implication of the above relation is similar to equation (5).

## 5. AN ILLUSTRATIVE EXAMPLE

To demonstrate the characteristics of time-varying complex-valued signal by using the dWDs, a linear chirp (frequency sweep) signal is taken as an example here, which is given by

$$p(t) = 2\,e^{j30^\circ \sin(2\pi t/5{\cdot}12)}\,e^{j(\omega_1 t^2/2 + b_1 t)} + 0{\cdot}5\,e^{j10^\circ \sin(2\pi t/5{\cdot}12)}\,e^{-j(\omega_1 t^2/2 + b_1 t)} + e^{j35{\cdot}16^\circ t}\,e^{j(\omega_2 t^2/2 + b_2 t)} + 1{\cdot}5\,e^{-j(\omega_2 t^2/2 + b_2 t)}, \tag{24}$$

with $\omega_1 = 8\pi$, $\omega_2 = 16\pi$, $b_1 = 6\pi$, $b_2 = 12\pi$. The signal was sampled at 100 Hz and the 512 complex valued data was processed to calculate the dWDs. Figure 2 shows the contour plots of the conventional auto-WD and auto-dWD with the same contour levels. Note that the conventional auto-WD is contaminated not only by the interference terms between forward and backward components, but by the interference terms between signal terms, whereas the auto-dWD shows only the interference terms between signal terms. As shown in Figure 3(a), the smoothed auto-dWD gives not only the accurate variation of the signal frequency with time but also the shape and directivity of the elliptic motions associated with each harmonic components in the complex plane. Figure 3(b) shows the SDI values associated with the fundamental and second harmonic components. Note that the second harmonic component forms a backward, thin elliptic planar motion, since its SDI value is about $-0{\cdot}2$. Figure 3(c), which was computed from the phase of the smoothed cross-dWD, represents the inclination angles of the instantaneous elliptic motions associated with the two harmonic components. The errors in results near the beginning and end portions of the signal are mainly caused by the short length of the estimated time-dependent Wigner kernel.

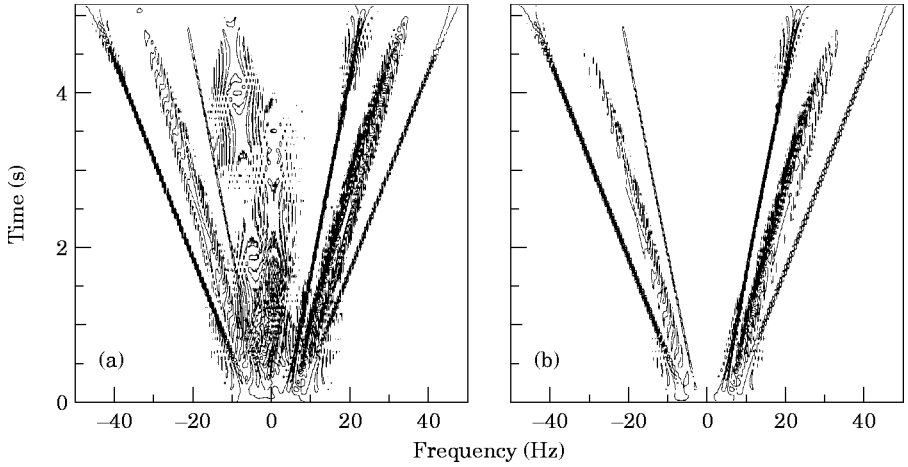


Figure 2. Conventional (a) and directional auto-WDs (b) of complex-valued linear chirp signal; $f_S = 100$ Hz; $N = 512$.

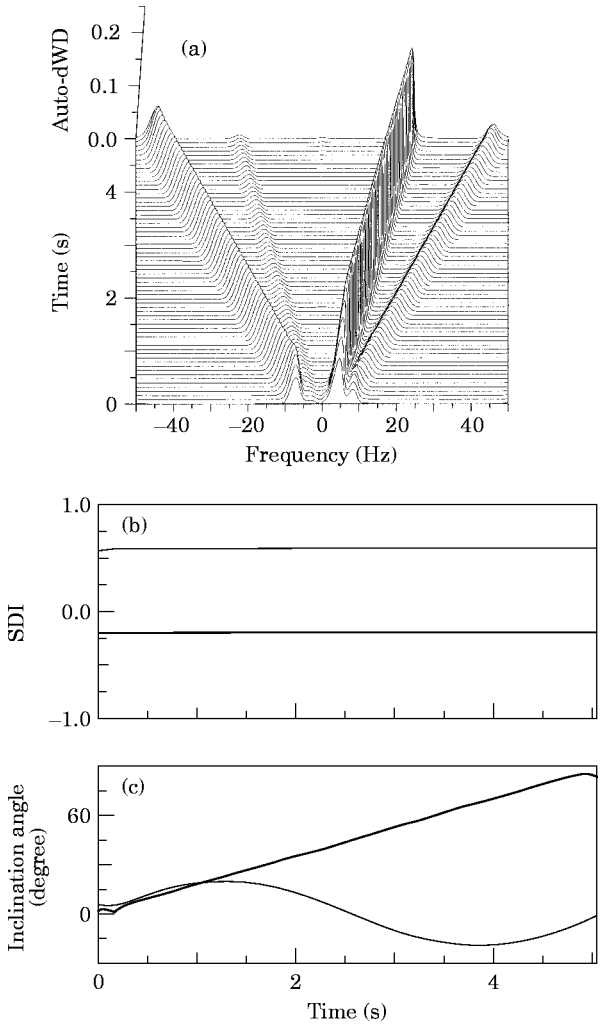


Figure 3. (a) Smoothed auto-dWD, (b) SDI and (c) inclination angle of complex-valued linear chirp signal; $f_S = 100$ Hz; $N = 512$; $\sigma_t = 20\Delta_t$; $\sigma_\omega = 20\Delta_\omega$. Key: ——, first component; ——, second component.

## 6. APPLICATION OF dWD TO ROTOR RUN-UP TEST

An anisotropic rotor system possesses the non-axisymmetric properties in its supporting stationary structure. The anisotropy in stiffness and damping of the support is known to produce elliptic whirl due to imbalance, which may be forward (the same direction as the rotor rotation) or backward (the opposite direction to the rotor rotation) [15]. With light damping, the synchronous backward whirl often occurs when the rotor system is operated between two very closely spaced resonant speeds. It makes the shaft undergo two reversals in stress per revolution, so that it may significantly contribute to shaft fatigue. Consequently, in anisotropic rotor systems, it is important to identify the backward whirl between the two split critical speeds.

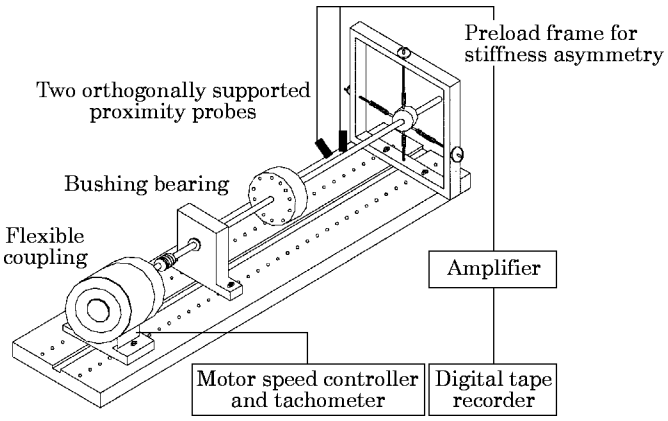


Figure 4. Experimental setup for rotor run-up test.

One of the most common ways to check the synchronous whirling direction, is to run the rotor at a constant speed, while the rotor speed is incremented by a fixed amount. Thus it requires many repeated test runs. Another quick test method is the use of the automatically tuned filter to the rotor speed during run-up or coast down. However, as the sweep rate increases, the spectral bandwidth increases and the frequency resolution decreases. As an alternative, use of smoothed dWD of transient complex signal during run-up is proposed to identify the backward synchronous whirl including the shape and inclination angle of the whirl orbit.

Figure 4 is the schematic of the laboratory test rig (Bently Nevada rotor kit: Model 24755). The test rig consists of one rigid disk and two bearing support pedestals. The outboard pedestal uses a preload frame to generate the stiffness

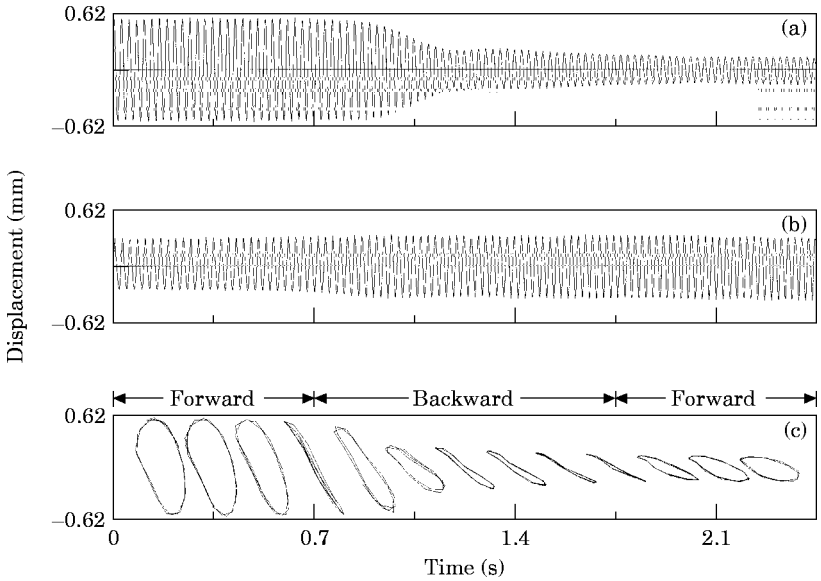


Figure 5. Vibration signals and whirl orbits of rotor during sweeping up from 2200 r.p.m. to 2460 r.p.m. with a constant acceleration rate. (a) $y$-axis; (b) $z$-axis; (c) whirling orbits.

asymmetry effect in the rig. The lateral vibrations adjacent to the outboard pedestal are measured by a pair of eddy current type proximity probes. The rotor system is driven by an electric motor incorporated with the tacho feedback through a flexible coupling. The recorded signals are filtered prior to A/D conversion using the low-pass filters with a nominal cut-off frequency of 200 Hz, and then sampled at a rate of 400 Hz. Each data set consists of 1024 data points.

Figure 5 shows the displacement–time histories and the whirl orbits in the neighborhood of the two critical speeds, when the rotating speed of the rotor is swept up from 2200 r.p.m. to 2460 r.p.m. with a constant acceleration rate. The time histories show that the $y$-axis critical speed is lower than the $z$-axis critical speed, so that the $y$ displacement reaches its maximum amplitude first. Whirl orbits

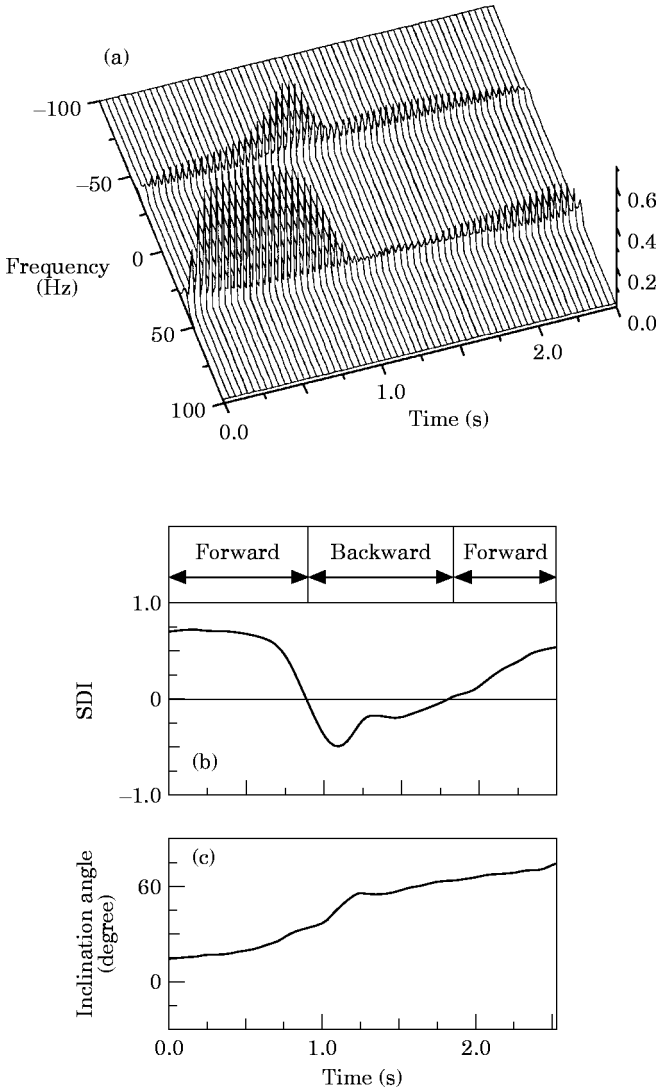


Figure 6. Rotor run-up test; $f_S = 400$ Hz; $N = 1024$; $\sigma_t = 20\Delta_t$; $\sigma_\omega = 20\Delta_\omega$. (a) Smoothed auto-dWD; (b) SDI of IX component; (c) Inclination angle of IX component.

versus running time show the presence of the backward whirl between 0·7 s and 1·75 s. Especially, at about 0·7 s running time, the orbits are collapsed into a straight line. At higher speeds, the whirl orbit begins to collapse again at about 1·75 s. These events are necessary for the change of whirling direction from the continuity point of view. It can also be seen from the whirl orbits that the major axis of orbits becomes inclined increasingly from the $y$-axis to the $z$-axis.

Figure 6 shows the smoothed auto-dWD, and the instantaneous SDI and inclination angle of 1X (synchronous to the rotational speed) component. It can be seen that the smoothed auto-dWD in Figure 6(a) well represents the time for backward whirl, its frequency components, and the shape of the instantaneous orbit. The smoothed auto-dWD shows that the two critical speeds are in the neighborhood of 2280 r.p.m. and 2390 r.p.m., respectively. SDI in Figure 6(b) clearly shows the shape and directivity of the instantaneous whirling orbit, and Figure 6(c) represents the instantaneous angle of 1X component made by the major axis of the orbits with $y$-axis. As shown in the time histories, response signals contain almost mono-component, that is, synchronous component, because the rotor operates at the neighborhood of critical speeds. Thus the resulting smoothed dWDs have little effects of the interference terms between multiple harmonic components, and make interpretation effective.

## 7. APPLICATION OF dWD TO TRANSIENT ENGINE VIBRATION TEST

A point of interest on an engine in operation will generally vibrate in three-dimensional space, making a complicated trajectory. The projected trajectory on an arbitrary plane can then be properly defined as a complex-valued signal. The dWD of the transient complex-valued signal representing the instantaneous planar motion, is utilized to characterize the transient engine vibration.

Experiments were carried out using a vehicle equipped with a four-stroke four-cylinder in-line spark ignition engine. The engine was run long enough to achieve steady state before the test. A triaxial accelerometer positioned at the

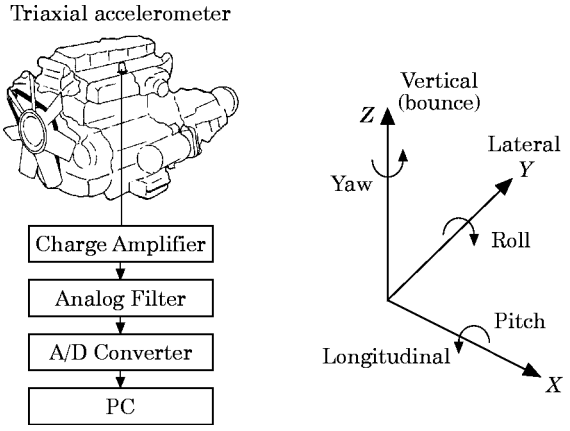


Figure 7. Experimental set-up and the co-ordinate system for engine vibration test.

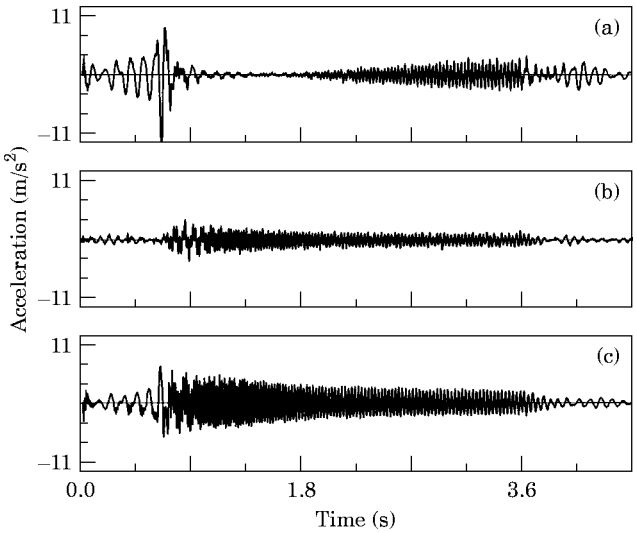


Figure 8. Trajectories of the transient engine vibrations during the crank-on/idling/engine-off. (a) Longitudinal, $x$ direction; (b) lateral, $y$ direction; (c) vertical (bounce), $z$ direction.

midpoint of the top of the engine block was used to measure the vibrations in the three perpendicular directions, $x$, $y$ and $z$, as shown in Figure 7. The vibration signals were low-pass filtered to prevent the aliasing and subsequently sampled at a rate of 220 Hz through a 12-bit A/D converter. The transient engine vibration signal was obtained during crank-on/idling/engine-off, where each data set consists of 1024 data points.

An engine body is generally treated as a rigid body with six-degree-of-freedom motions, consisting of the longitudinal, lateral and vertical (bounce) motions and the roll, pitch and yaw motions, as shown in Figure 7. With the measurement in the $x$, $y$ and $z$ directions, one can define three different planar motions, one of which can always be regenerated from the other two. For the sake of convenience, only the rolling planar motion is dealt with by introducing the complex-valued signal $r(t) = z(t) + \mathrm{j}x(t)$.

Figure 8 shows the transient engine vibrations during crank-on/idling/engine-off. The time histories show not only an abrupt shake of typical engine body during crank-on and engine-off but also some idling state. This figure shows that the vertical (bounce) and longitudinal vibrations are larger than the lateral vibration. Figure 9

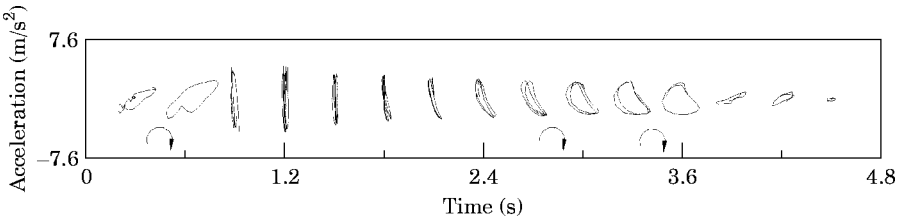


Figure 9. Trajectories of the transient engine vibrations during the crank-on/idling/engine-off. Frontal plane ($r = z + \mathrm{j}x$).

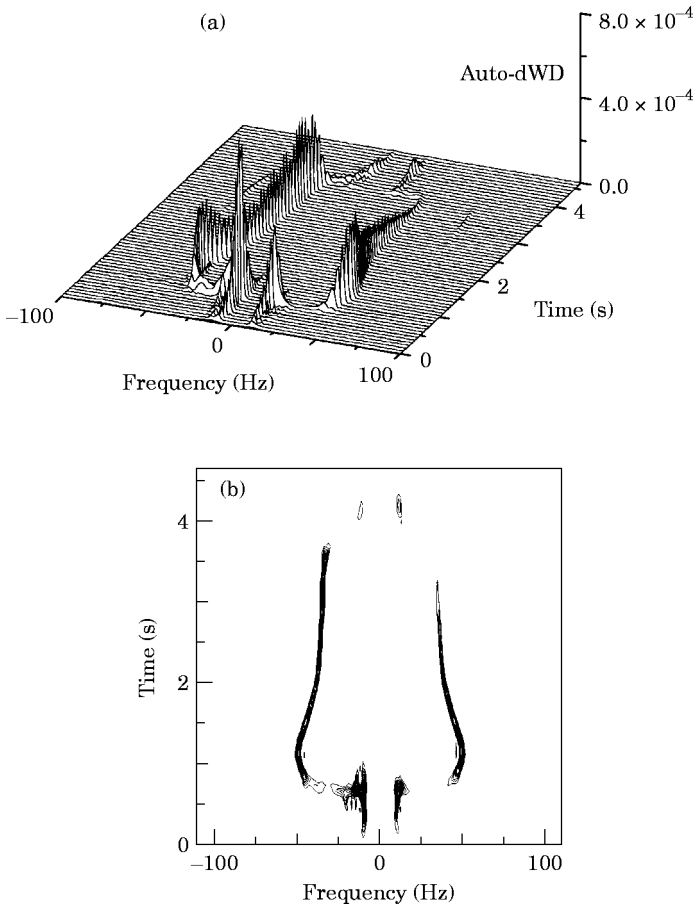


Figure 10. Smoothed auto-dWD of the transient engine vibrations during the crank-on/idling/engine-off; $f_S = 220$ Hz; $N = 1024$; $\sigma_t = 10\Delta_t$; $\sigma_\omega = 10\Delta_\omega$. Frontal plane ($r = z + jx$): (a) waterfall plot; (b) contour plot.

shows the instantaneous trajectories of the transient engine vibrations in Figure 8. The rotation direction of trajectories shown in Figure 9 indicates the rotation direction of the crank shaft. Although the trajectories indicate the shape, directivity, and inclination angle of the instantaneous planar motion, they do not give accurate information of the variation of the signal frequency with time.

In order to track the shape and directivity of the transient engine vibration, the resulting three-dimensional waterfall and the contour plots of smoothed auto-dWD are displayed in Figures 10(a) and 10(b), respectively. These figures show that as soon as crank-on ends, the engine speed jumps up to about 1500 r.p.m., and then slowly decreases down to the idling speed of 820 r.p.m. Figure 11 shows the instantaneous SDI and inclination angle of the motion synchronous to firing frequency, which was readily obtained from the auto-dWD and cross-dWD, respectively. The same results may also be obtained directly from Figure 9, but the calculation is quite involved. Note that the inclination angle as well as the vibration amplitude abruptly change at the onset of engine-off.

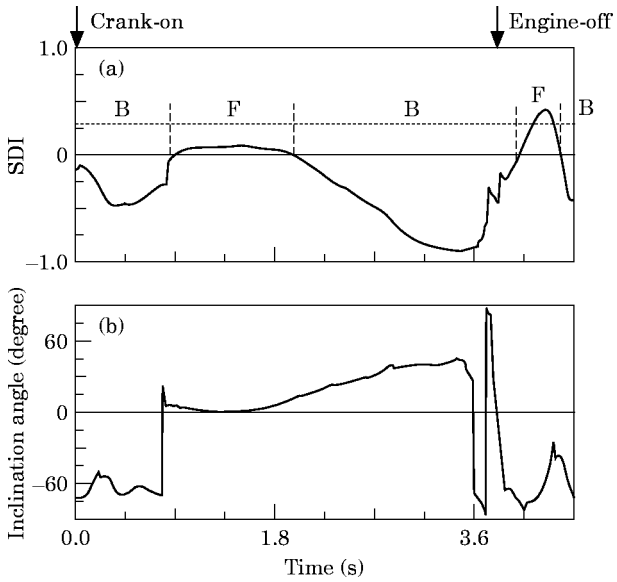


Figure 11. (a) Instantaneous SDI and (b) inclination angle of the dominant transient engine vibration during the crank-on/idling/engine-off by smoothed dWDs; $f_S = 220$ Hz; $N = 1024$; $\sigma_t = 20\Delta_t$; $\sigma_\omega = 20\Delta_\omega$. F, Forward; B, backward.

## 8. CONCLUSIONS

Transient vibration signal processing method is proposed utilizing auto- and cross-dWDs of time-varying complex-valued signal representing the instantaneous planar motion. The experimental results for characterization of time-varying complex-valued signals show that the shape, directivity, and inclination angle of instantaneous planar motion can be effectively identified by using the smoothed auto-and cross-dWDs, respectively.

## ACKNOWLEDGMENT

The authors would like to acknowledge the support of the Bently Nevada Corporation by providing the rotor kit.

## REFERENCES

1. L. COHEN 1995 *Time–Frequency Analysis*. New York: Prentice Hall; pp. 113–135.
2. T. A. C. M. CLAASEN and W. F. G. MECKLENBRAUKER 1980 *Philips Journal of Research* **35**, 217–250 (Part I), 276–300 (Part II), 372–389 (Part III). The Wigner distribution—a tool for time–frequency signal analysis.
3. F. HLAWATSCH and G. F. BOUDREAUX-BARTELS 1992 *IEEE Signal Processing Magazine* **9**, 21–67. Linear and quadratic time–frequency signal representations.
4. S. QIAN and D. CHEN 1996 *Joint Time–Frequency Analysis*. New York: Prentice Hall; pp. 113–135.
5. L. COHEN 1992 *Time–Frequency Signal Analysis*: *Methods and Applications* (B. Boashash, editor). Longman Cheshire. Introduction: a primer on time–frequency analysis, pp. 3–42.

6. H. O. Bartelt, K. H. Brenner and A. W. Lohmann 1980 *Optics Communications* **32**, 32–38. The Wigner distribution function and its optical production.
7. M. Riley 1992 *Speech Time–Frequency Representations*. Kluwer Academic Publishers.
8. T. J. Wahl and J. S. Bolton 1993 *Journal of Sound and Vibration* **163**, 101–122. The application of the Wigner distribution to the identification of structure-borne noise components.
9. N. Yen 1987 *Journal of Acoustical Society of America* **81**, 1841–1850. Time and frequency representation of acoustic signals by means of the Wigner distribution function: implementation and interpretation.
10. Q. Meng and L. Qu 1991 *Mechanical Systems and Signal Processing* **5**, 155–166. Rotating machinery fault diagnosis using Wigner distribution.
11 P. D. McFadden and W. J. Wang 1992 *Institute of Mechanical Engineers* C432/134, 387–393. Analysis of gear vibration signatures by the weighted Wigner–Ville distribution.
12 J. Leuridan, H.V.D. Auweraer and H. Vold 1994 *Sound and Vibration* **11**, 14–26. The analysis of nonstationary dynamic signals.
13. Y. S. Shin and J. J. Jeon 1993 *Shock and Vibration* **1**, 65–76. Pseudo Wigner–Ville time–frequency distribution and its application to machinery condition monitoring.
14. A. H. Nuttal 1989 *Naval Underwater Systems Center*: *Technical Report TR*8533. Alias-free Wigner distribution function and complex ambiguity function for discrete-time samples.
15. C. W. Lee 1993 *Vibration Analysis of Rotors*. Kluwer Academic Publishers; pp. 40–48.
16. C. W. Lee, J. P. Park and Y. S. Han 1995 *Fifteenth Biennial ASME Conference on Vibration and Noise* **3**, Part A, DE-84-1, 1397–1403. Use of directional AR and ML spectra for detection of misfired engine cylinder.
17. C. W. Lee, Y. S. Han and J. P. Park 1995 *Asia-Pacific Vibration Conference*, 617–622. Detection of engine cylinder power fault by using directional power spectra of vibration signals.
18. R. B. Randall 1987 *Frequency Analysis*. Denmark: Brüel and Kjaer; third edition, pp. 58–77.
19. F. Hlawatsch, T. G. Manickam, R. L. Urbanke and W. Jones 1995 *Signal Processing* **43**, 149–168. Smoothed pseudo-Wigner distribution, Choi–Williams distribution and cone-kernel representation: ambiguity-domain analysis and experimental comparison.
20. N. D. Cartwright 1976 *Physica* **83A**, 210–212. A non-negative Wigner-type distribution.